Proc. Indian Acad. Sci. (Earth Planet. Sci.), Vol. 101, No. 2, June 1992, pp. 153–176.

On the stability of a coupled ocean atmosphere system in the presence of wave-CISK

SUDHA SELVARAJAN* and B N GOSWAMI

Centre for Atmospheric Sciences, *Aerospace Engineering Department, Indian Institute of Science, Bangalore 560012, India

MS received 19 July 1991; revised 17 March 1992

Abstract. The stability of a simple coupled ocean-atmosphere system similar to the one studied by Hirst with general ocean thermodynamics is investigated in which the atmospheric heating is determined by sea surface temperature anomalies as well as the convergence feedback (low level moisture convergence by the waves themselves). It is shown that the unstable coupled mode found by Hirst (UH mode) is profoundly modified by the convergence feedback. The feedback increases the unstable range of the UH mode and can increase its growth rate several folds. The maximally growing UH mode can become westward propagating for certain strength of convergence feedback. If the convergence feedback strength exceeds a critical value, several new unstable intraseasonal modes are also introduced. These modes are basically 'advective' modes. For relatively weak strengths of the convergence feedback the growth rates of these modes are smaller than that of the UH mode. As the atmosphere approaches 'moist neutral' state, the growth rates of these modes could become comparable or even larger than that of the UH mode. It is argued that these results explain why the El Nino and Southern Oscillation (ENSO) signal is clear in the eastern Pacific but not so in the western Pacific and they may also explain some of the differences between individual ENSO events. Our results also explain the aperiodic behaviour of some coupled numerical models. Importance of this process in explaining the observed aperiodicity of the ENSO phenomenon is indicated.

Keywords. Large scale air-sea interactions; coupled instability; wave-CISK; ocean-atmosphere system; atmospheric heating; convergence feedback

1. Introduction

Although the linear tropical atmosphere and the tropical ocean may be independently stable, coupling between them can introduce unstable coupled modes (Philander *et al* 1984; Hirst 1986; Rennick and Haney 1986; Yamagata 1985; Lau and Shen 1988). Such unstable air-sea interactions have played a crucial role in the evolution of the delayed oscillator mechanism for the El Nino and Southern Oscillation (Suarez and Schopf 1988; Battisti and Hirst 1989) phenomenon (ENSO). They are also important for the predictability of the coupled system (Goswami and Shukla 1991a). Study of necessary conditions for instability (Yamagata 1985; Hirst 1986) shows that ocean perturbations can grow only if positive correlations exist between the ocean currents and the atmospheric surface winds (U, u and/or V, v). Thus it depends on the structure of the eigenfunctions of a particular coupled normal mode. Hirst (1986, hereafter referred to as H86) showed that the structure of the coupled eigenfunctions depends crucially on the oceanic thermodynamic processes. In the upwelling-dominated case, the structure of the Kelvin wave was such that the surface winds and the ocean currents could

cooperate. However, in the advection-dominated case the structure of the Kelvin wave changed to the extent that the surface winds and the ocean currents were uncorrelated and the wave was damped. In this case the eigenfunctions for the $n = 1$ Rossby mode were modified so that this mode became unstable. This explained the apparently contradictory results between some early studies (Philander *et al* 1984; Rennick and Haney 1986). Whether upwelling or advection would dominate the ocean thermodynamics depends on the prevailing mean conditions. Rough estimates (Hirst 1986; Battisti and Hirst 1989) indicate that while upwelling may dominate in the eastern Pacific, advection may dominate in the western Pacific. In the central Pacific, both these processes may be important.

All the studies on coupled instability with the exception of Lau and Shen (1988), assume that the atmospheric heating is directly proportional to the sea surface temperature (SST) anomaly. This simple-minded parametrization of the atmospheric heating assumes that the tropical ocean is warm and an increase in SST increases evaporation. This increase in available moisture then results in increase in condensation and heating through convective instability. Modelling studies (e.g., Shukla and Wallace 1983; Fennessy *et al* 1985) show that local evaporation accounts for only about a quarter of the precipitation anomalies while the remaining three quarters of the precipitation anomalies come from large scale low-level convergence. Organized heating of the atmosphere results in low-level convergence of moisture to the heating region. This leads to increased moisture flux to the heating region and further enhancement of the heating. Several studies (Webster 1981; Zebiak 1982) have shown that this mechanism (hereafter referred to as the convergence feedback) enhances atmospheric heating. In the present study, it is argued that convergence feedback is an important process in the tropical dynamics and the stability of the coupled system could not be studied without the inclusion of this process. Inclusion of this process in the parameterization of atmospheric heating modifies the atmospheric heating and hence the structure of eigenfunctions of the coupled modes. In the simplest form of parameterization, this process results in a reduction of the effective static stability of the atmosphere. This results in reduction of the phase speed of the atmospheric waves. If convergence feedback reduces the atmospheric static stability sufficiently, the phase speed of some of the atmospheric waves may be comparable to the phase speed of some oceanic waves. This introduces the possibility of strong coupling between the two systems. Lau and Shen (1988) studied the effect of convergence feedback on coupling between atmospheric Kelvin wave and the oceanic Kelvin wave. This essentially excludes the effect of the Coriolis force. Moreover, they studied the non- dissipative case. The growth rate of their coupled mode is smaller than the atmospheric dissipation rates used in many coupled model studies. Therefore, it is unlikely that the coupled modes seen by Lau and Shen (1988) would play any significant role in the real coupled system. In this study, we examine the effect of convergence feedback on a more complete coupled system including the effect of Coriolis force (equatorial β plane). It is shown that this allows many new modes to be unstable and drastically modifies the character of the most unstable mode in H86.

Hirst and Lau (1990), also recently studied the stability of the coupled system in which the convergence feedback (wave-CISK) contributes to the atmospheric heating. However, they restricted their study to either 'advective' or to the 'upwelling' limits of

the ocean thermodynamics only. Moreover, they consider only cases when the atmospheric gravity wave speed is very close to or smaller than the oceanic gravity wave speed. This means that the effective atmospheric stability is very close to moist neutral ($\leqslant 0{\cdot}5\%$ of the dry static stability) case. This is a rather very special situation. Our study differs from that of Hirst and Lau in two important ways. First, we consider the general oceanic thermodynamic case (model III of H86). While the 'advective' and the 'upwelling' limits are useful limits for understanding the dynamics, as shown by H86, the general thermodynamic case is fundamentally different and may be more relevant to the dynamics of ENSO events. Second, we show how the unstable modes evolve with variation of effective atmospheric static stability over a wide range of values. A brief summary of some preliminary results of this study has appeared in Goswami and Selvarajan (1991). The present work contains a comprehensive account of the role of the wave-CISK on the coupled instability with additional new results and insights.

2. Model details

The coupled system comprises of a linear first baroclinic mode atmosphere and a linear reduced gravity ocean interacting through (i) stresses parametrized in terms of atmospheric winds and (ii) atmospheric heating parameterized in terms of convergence feedback and SST anomaly fields. This model is similar to model III used in H86 except that the atmospheric heating is now parametrized in terms of convergence feedback and sea surface temperature anomaly field. In the coupling parametrization of H86 the atmospheric heating was assumed to be proportional to sea surface temperature anomaly field only.

2.1 *The ocean model*

The equations for the oceanic perturbations are given by

$$u_t - \beta y v + \alpha g \overline{\Delta T} h_x + a u = \tau^x/(\rho_0 \bar{h}), \tag{1a}$$

$$v_t + \beta y u + \alpha g \overline{\Delta T} h_y + a v = \tau^y/(\rho_0 \bar{h}), \tag{1b}$$

$$h_t + \bar{h}(u_x + v_y) + bh = 0, \tag{1c}$$

$$T_t + u \bar{T}_x - K_T h + dT = 0. \tag{1d}$$

These equations represent an ocean model consisting of a mixed layer with a deep, cold, inert layer below it. A thin thermocline separates the two layers. Motion and temperature are assumed to be constant with depth in the mixed layer. The dependent variables $(u, v, h, T, \tau^x, \tau^y)$ represent perturbations in zonal current, meridional current, thermocline depth, temperature, zonal windstress and meridional windstress. $\overline{\Delta T}$ is the difference between the temperatures in the mixed layer and the deep layer and $\bar{h}$ is the mean thermocline depth. a is the coefficient of Rayleigh friction and b,d are that of Newtonian cooling for the ocean. This model is similar to the oceanic component of model III of H86.

2.2 *The atmosphere model*

The equations for the atmospheric perturbations are given by,

$$U_t - \beta y V - (gH/\theta_0)\theta_x + AU = 0, \tag{2a}$$

$$V_t + \beta y U - (gH/\theta_0)\theta_y + AV = 0, \tag{2b}$$

$$\theta_t - (C_a^2\theta_0/gH)(U_x + V_y) + B\theta = -Q_{\text{conv}} - (\theta_0/gH)K_Q T, \tag{2c}$$

$$q_t + q_0(U_x + V_y) = E - P. \tag{2d}$$

θ is the potential temperature perturbation at the mid-level. This model can be derived from the atmospheric component of model III of H86 by using the relation

$$\phi = -(gH/\theta_0)\theta, \tag{3}$$

where ϕ is the geopotential thickness (Davey and Gill 1987). θ_0 is the mean background temperature at mid-level and H the scale height. It is to be noted that the mass source/sink term in the ϕ equation of model III of H86 has a negative sign as U, V in this model are interpreted as upper layer winds. This leads to negative signs of the heating terms in our θ equation. Equation (2d) represents a linearized moisture balance where q is the perturbation moisture content, E the surface evaporation and P the precipitation anomaly. To a first order of approximation it can be assumed that the atmosphere can be divided into two different heating regimes, namely, the convective regime and the non-convective regime. In the convective regime, when q increases, since the atmosphere remains saturated $q_t = 0$ and the extra moisture gained by convergence and evaporation is depleted as precipitation. Hence from (2d) we get,

$$q_{\text{os}}(U_{lx} + V_{ly}) = E - P, \tag{4}$$

where q_{os} is the background saturated moisture content. In this regime, heating occurs by condensation only and so $q = q_0 = q_{\text{os}}$. In the non-convective regime, $P = 0$ and the evaporated and converged moisture goes into moistening the atmosphere. It is assumed that tropical atmosphere is always saturated and is in a state that can be categorized as convective regime.

In the convective regime, the heating rate Q_{conv} associated with wave convergence is related to precipitation by

$$Q_{\text{conv}} = \frac{\rho_w L_v}{H_0 \rho_a C_p} P_{\text{conv}}. \tag{5a}$$

The background saturated moisture content q_{os} is a strong function of SST through the Clausius-Clapeyron equation. Assuming a standard lapse rate of the tropical atmosphere of $\tilde{\Gamma} = 6{\cdot}5°\text{C/km}$, and that the temperature at the interface of air-sea remains a constant one can linearize the Clausius-Clapeyron equation to give

$$q_{\text{os}}(T_s) \approx \bar{q} \exp[0{\cdot}059(T_s - 301)]$$

$\bar{q}$ is the saturated moisture at 301 K and has the value of 7·2 cm (Lau and Shen 1988).

The heating term in the atmosphere model consists of two parts, namely, Q_T and Q_{conv}. The part $Q_T = (\theta_0/gH)\, K_Q T$ is the same as used by H86 and is contained in

the term E. It represents heating of the atmosphere by increase in local evaporation due to increase in SST. The term Q_{conv} represents heating due to low-level wave convergence. Since the increase in atmospheric heating from local evaporation due to increase in SST (i.e., Q_T term) is considered separately, the precipitation due to low-level convergence may be represented as

$$P_{\text{conv}} = -q_{\text{os}}(U_{lx} + V_{ly}). \tag{5b}$$

Substituting in (5a) for P_{conv} from (5b) we obtain

$$Q_{\text{conv}} = -\frac{L_v \rho_w}{H_0 C_p \rho_a} q_{\text{os}} \left[\frac{\partial U_l}{\partial x} + \frac{\partial V_l}{\partial y}\right]$$

$$= \frac{L_v \rho_w}{2H_0 C_p \rho_a} q_{\text{os}} \left[\frac{\partial U}{\partial x} + \frac{\partial V}{\partial y}\right], \tag{6}$$

where the low-level winds (U_l, V_l) are given by

$$(U_l, V_l) = -(U, V)/2,$$

q_{os} represents the saturated moisture corresponding to a background mean SST T_s expressed in units of depth of precipitable water. H_0 is a projection factor and is $\approx 2H$ (Davey and Gill 1987) if all the latent heat is assumed to go to the first baroclinic mode. With these parameterizations, (2c) may be rewritten as

$$\frac{\partial \theta}{\partial t} - \frac{C_a^2 \theta_0}{gH}\left[\frac{\partial U}{\partial x} + \frac{\partial V}{\partial y}\right](1 - q_s) + B\theta = -\frac{\theta_0}{gH} K_Q T, \tag{7}$$

where T is the SST perturbation and $q_s = q_{\text{os}}/q_{\text{crit}}$, with $q_{\text{crit}} = 2C_p \rho_a H_0 C_a^2 \theta_0/(L_v \rho_w g H)$. With $\theta_0 = 310°\text{K}$, q_{crit} is approximately 7·6 cm.

2.3 *Method of solution*

As in H86 the wind stresses are parameterized in terms of the atmospheric low level winds.

$$(\tau_x, \tau_y) = \gamma(U, V).$$

The method of non-dimensionalization is exactly the same as in H86 except that θ is non-dimensionalized with $C_a \theta_0/gH$. Values of the parameters used are given in table 1. The non-dimensional equations of the coupled system are given by

$$u_t - yv + h_x + au = K_S U, \tag{8a}$$

$$v_t + yv + h_y + av = K_S V, \tag{8b}$$

$$h_t + \bar{h}(u_x + v_y) + bh = 0, \tag{8c}$$

$$T_t + u\bar{T}_x - K_M h + \mathrm{d}T = 0, \tag{8d}$$

$$U_t - yV - \theta_x + AU = 0, \tag{8e}$$

$$V_t + yU - \theta_y + AV = 0, \tag{8f}$$

$$\theta_t - C^2(U_x + V_y)(1 - q_s) + B\theta = -\hat{K}_Q T, \tag{8g}$$

where $C^2 = C_a^2/C_0^2$ and $\hat{K}_Q = K_Q \overline{\Delta T} t_0/C_0^2$ and the other non-dimensional parameters are same as those used in H86.

Table 1. Values of the constants used in the *standard* case.

Parameter	Dimensional value	Non-dimensional value
C_0	$1{\cdot}4\,\mathrm{ms}^{-1}$	1·0
L_0	$250 \times 10^3\,\mathrm{m}$	1·0
t_0	$1{\cdot}8 \times 10^5\,\mathrm{s}$	1·0
a, b, d	$1{\cdot}16 \times 10^{-7}\,\mathrm{s}^{-1}$	$0{\cdot}2049 \times 10^{-1}$
C_a	$30\,\mathrm{ms}^{-1}$	25·0
A, B	$5{\cdot}0 \times 10^{-6}\,\mathrm{s}^{-1}$	$0{\cdot}7771 \times 10^{-1}$
K_Q	$7{\cdot}0 \times 10^{-3}\,\mathrm{m^2 s^{-3} K^{-1}}$	$0{\cdot}3091 \times 10^{-2}$
K_S	$8{\cdot}0 \times 10^{-8}\,\mathrm{s}^{-1}$	$0{\cdot}1413 \times 10^{-1}$
K_T	$3{\cdot}5 \times 10^{-9}\,\mathrm{km^{-1} s^{-1}}$	$0{\cdot}88 \times 10^{4}$
$\bar{T}_x$	$-5{\cdot}0 \times 10^{-7}\,\mathrm{km}^{-1}$	$-0{\cdot}8831 \times 10^{-2}$
$\bar{T}_y$	$-3{\cdot}053 \times 10^{-7}\,\mathrm{km}^{-1}$	$-0{\cdot}3053 \times 10^{-3}$
$\bar{h}$	70 m	—
$\overline{\Delta T}$	14 K	—

The meridional dependence of amplitudes (U, V, ϕ, u, v, h, T) are then expressed in terms of the sum of parabolic cylinder functions as

$$S(y) = \sum_{n=0}^{N} S_n D_n(y),$$

where D_n is the parabolic cylinder function. The selection of parabolic cylinder functions is most appropriate since they form the basis functions for the normal modes of an ocean or an atmosphere on an equatorial beta plane. Parabolic cylinder functions are orthogonal and thus equations (8) are transformed into a set of linear algebraic equations given by $MX = i\sigma X$ where M is a $7N \times 7N$ sparse matrix and $i\sigma$ and X are eigenvalues and eigenvectors. The series is truncated at $N = 20$ (Also see Appendix). The system of equations is solved using a standard technique with double precision.

2.4 *Energetics*

From the above set of non-dimensional equations an energy integral equation can be derived for the atmosphere and the ocean separately (Lau and Shen 1988; Hirst 1986). Multiply equations (8e) by U, (8f) by V, and (8g) by θ/Γ and sum over the terms to get

$$\partial E_a/\partial t = -AU^2 - AV^2 - (B/\Gamma)\theta^2 - (\hat{K}_Q/\Gamma)\theta T,$$

where $\Gamma = (1 - q_s)C_a^2/C_0^2$. Integrating over one wavelength in x and between $\pm\,\infty$ in y this equation can be written as

$$\partial\langle E_a\rangle/\partial t = -A\langle U^2\rangle - A\langle V^2\rangle - (B/\Gamma)\langle\theta^2\rangle - (\hat{K}_Q/\Gamma)\langle\theta T\rangle. \tag{9a}$$

Similarly, for the ocean the energy integral equation is

$$\partial\langle E_0\rangle/\partial t = -a\langle u^2\rangle - a\langle v^2\rangle - b\langle h^2\rangle - K_s\langle uU\rangle - K_s\langle vV\rangle. \tag{9b}$$

In (9) $E_a = (U^2 + V^2 + \theta^2/\Gamma)/2$ and $E_0 = (u^2 + v^2 + h^2)/2$ are measures of total energy of the atmospheric and oceanic perturbations and $\langle\rangle$ represents the integral over one

wavelength in x and between $\pm\ \infty$ in y. Equation (9) shows that the oceanic perturbations can grow only if the oceanic zonal currents (u) and atmospheric zonal winds, U (upper level winds in this model) and/or the oceanic meridional currents (v) and atmospheric meridional winds (v) are negatively correlated. Alternatively, if the lower layer zonal (meridional) winds correlate positively with oceanic zonal (meridional) currents, oceanic perturbations may grow. Similarly, atmospheric perturbations can grow only if the atmospheric temperature perturbation (θ) and SST perturbation (T) are negatively correlated.

4. Results and discussion

In the absence of convergence feedback ($q_s = 0$), this model is identical to the model III of H86 and the corresponding results were reproduced. For the standard set of parameters (listed in table 1) there is only one unstable mode whose maximum growth rate occurs for non-dimensional wavenumber $k = 0{\cdot}15$. The e-folding time and period of this eastward propagating mode at this wavelength are about 5 months and 26 months respectively (hereafter referred to as the UH mode). Now the effect of including the convergence feedback is studied. As q_s is increased the growth rate of this UH mode increases steadily and beyond a critical value of q_s new unstable modes start appearing. The number of new unstable modes increases steadily as q_s increases. The dispersion relation for the unstable modes for $q_s = 0{\cdot}8$ is shown in figure 1 and for $q_s = 0{\cdot}95$ is shown in figure 2. The symbols used to represent the various modes are consistent within the same figure and should not be compared with those of another figure. All the modes are identified in figure 1 and in figure 2 only the three gravest modes (i.e., UH, EM and WM) are prominently marked. It is to be noted that the new modes appear in two distinct sets, one set of eastward propagating modes and another set of westward propagating modes both roughly of the same period. Apart from the UH mode, the maximally growing eastward propagating mode is termed the EM mode and similarly the maximally growing westward propagating mode is designated as the WM mode. The labels E2, E3, E4 represent the other eastward propagating modes and W2, W3 represent the other westward propagating modes. Secondly, the growth rates of all the new modes seem to have only a very weak dependence on the wavenumber. At moderate strength of convergence feedback (e.g. $q_s = 0{\cdot}8$, figure 1) the UH mode is still the dominant mode with maximum growth rate for $k \approx 0{\cdot}15$ (wavelength $\approx$ 10,000 km). However, as q_s (or equivalently, the mean background SST) increases, its character gets modified drastically. From figure 2 it is seen that for $q_s = 0{\cdot}95$, the growth rates of some of the new modes are already comparable to that of the UH mode. Figure 3 shows the non-dimensional dispersion relation for the UH mode as a function of the strength of the convergence feedback (q_s). The unstable regime of the mode in the wavenumber domain also increases with increasing q_s. It is to be noted that with moderately strong convergence feedback, the growth rate of the UH mode has a maximum around $k \approx 0{\cdot}15$, facilitating a scale selection for this mode. It is seen that the eastward phase speed of the UH mode goes on decreasing until non-dimensional q_s is about 0·8 when it becomes nearly stationary. With further increase of q_s it becomes westward propagating. At $q_s = 0{\cdot}9$ the maximally growing UH mode is westward propagating and its period is about 20 months. However, at higher values of q_s its period further decreases and it becomes indistinguishable from the westward propagating

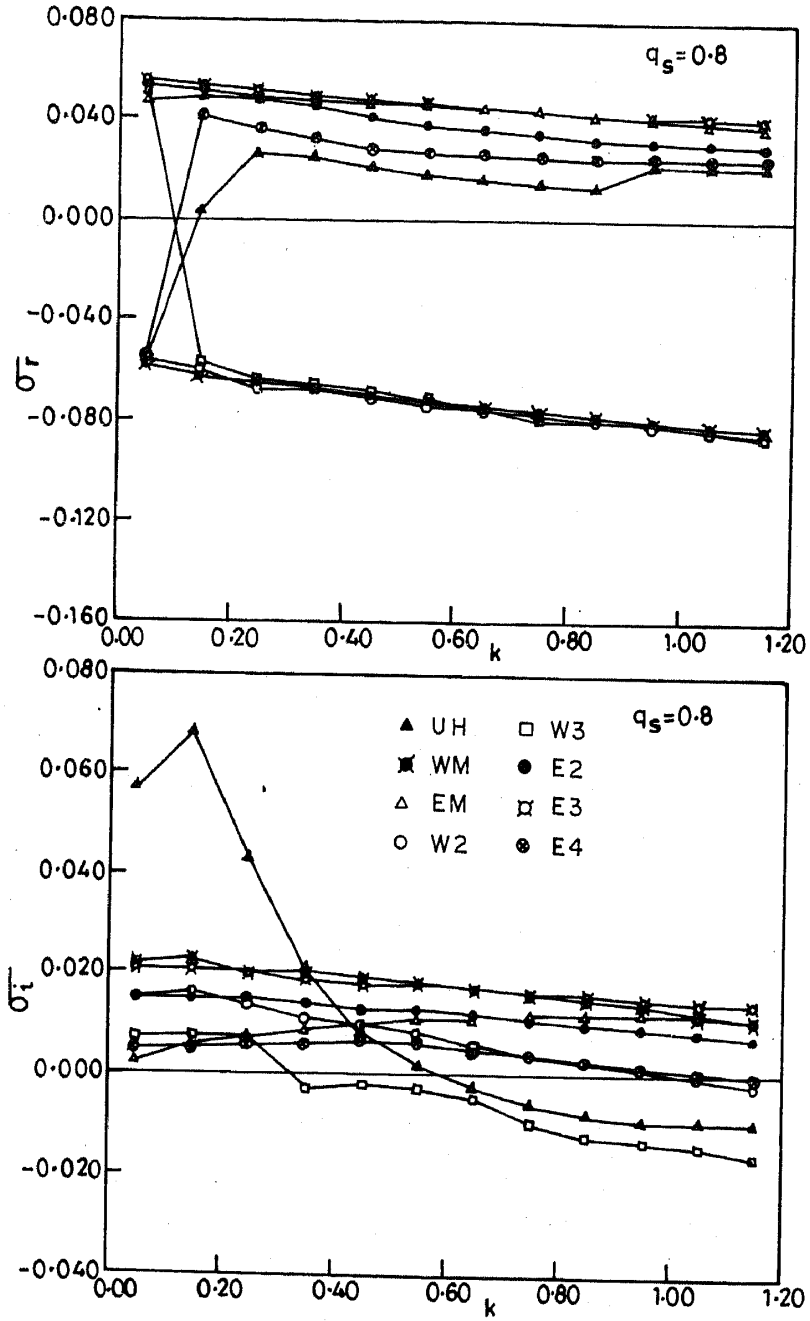

Figure 1. Non-dimensional dispersion relation (all modes) for $q_s = 0{\cdot}8$. σ_r, σ_i and k are the real frequency, imaginary frequency and wavenumber respectively. Other symbols are explained in the text.

intraseasonal modes. Decreasing q_s slowly we could trace the new unstable modes to be neutral interannual modes with periods greater than one year. In the presence of convergence feedback, periods of both the gravest new modes go on decreasing with increasing q_s. This character is similar to the character of the growth of the Kelvin mode found by Lau and Shen (1988) when background SST (T_s) exceeds a critical value of about 28°C. This character of dependence on q_s is seen for all wavelengths (i.e. all k). For $q_s > 0{\cdot}95$, the growth rates of some of the new unstable modes become comparable or even larger than that of the UH mode. The non-dimensional dispersion relation for the

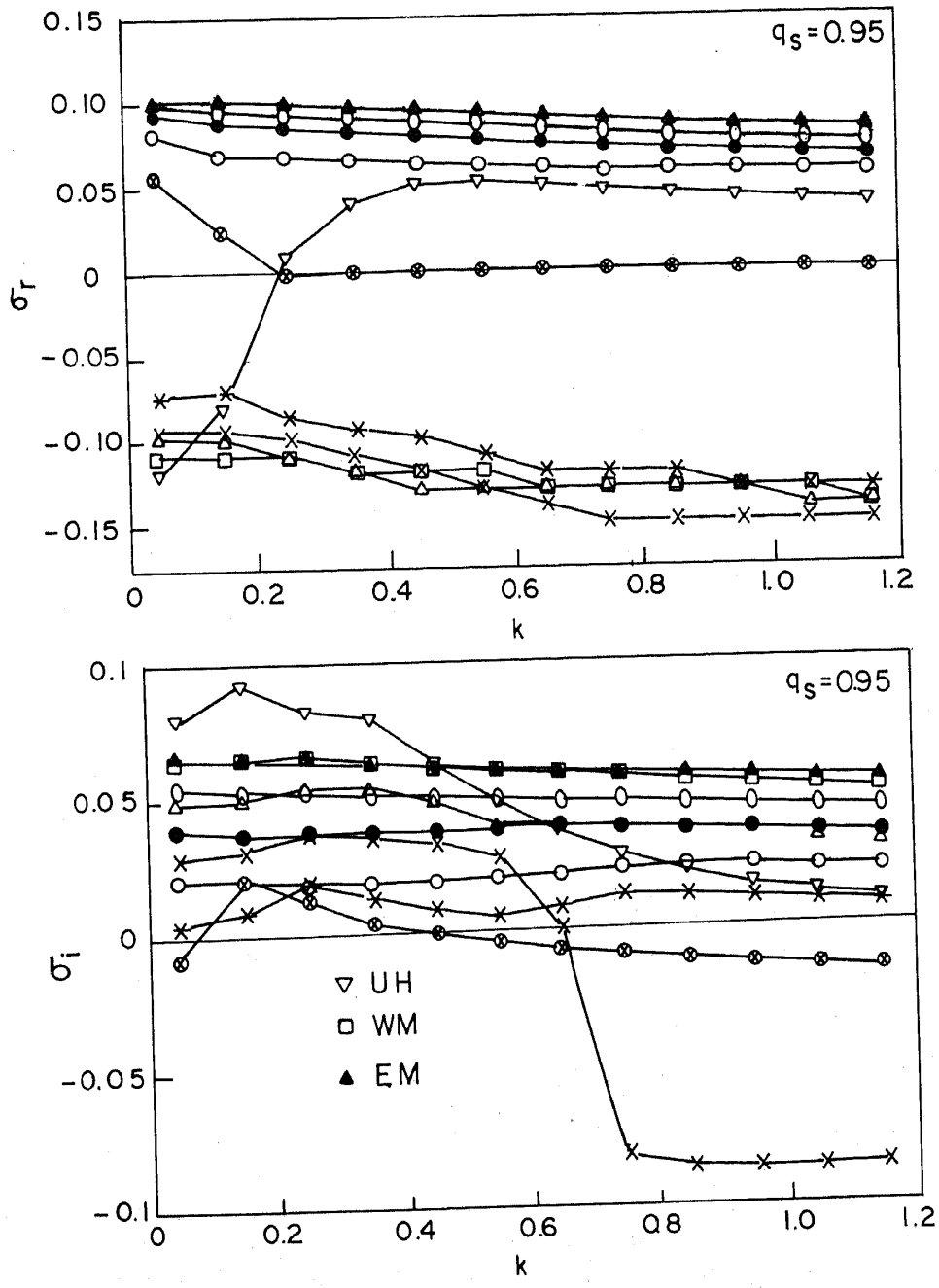

Figure 2. Same as in figure 1 but for $q_s = 0{\cdot}95$.

EM, WM modes as a function of q_s is shown in figure 4. It is clear that the eastward and westward propagating modes remain eastward and westward but their growth rates increase with increasing q_s. In order to provide a better idea of the dependence of the unstable modes on q_s, we show in figure 5 the variation in the period and e-folding time of all the unstable modes as q_s is increased from 0·0 to 0·98 for the wavenumber $k = 0{\cdot}15$. While the UH mode exists even if $q_s = 0$, the new unstable modes appear only when q_s exceeds a critical value. The e-folding time of the UH mode decreases (or the growth rate increases) with an increase in q_s. However, the period of the UH mode does not change appreciably until $q_s = 0{\cdot}6$ and then increases sharply until about $q_s \approx 0{\cdot}8$. At this strength of convergence feedback this mode is stationary (represented by a gap in

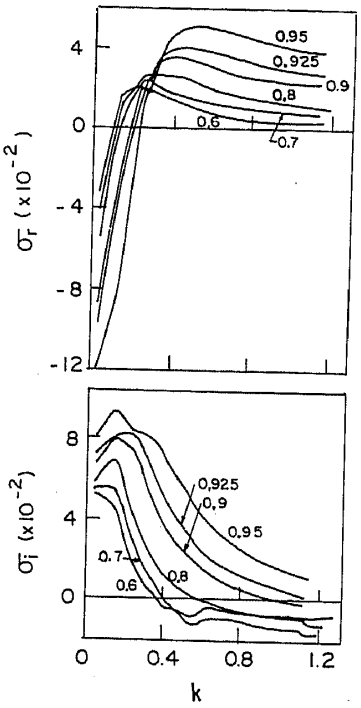

Figure 3. Non-dimensional dispersion relation for the UH mode for different strengths of convergence feedback (q_s).

the figure as the period becomes infinity) and with a further increase in q_s the period decreases sharply. However, it is to be noted that the direction of propagation is eastward for $q_s < 0{\cdot}8$ and westward for $q_s \geq 0{\cdot}9$. As q_s increases new unstable modes start appearing whose e-folding times and periods decreases rapidly. For larger values of q_s the e-folding time and period of all the modes are close to each other.

As discussed by Yamagata (1985) and H86 the stability characteristics of the unstable modes depend crucially on the product of the coupling coefficients i.e., $K_Q K_S$ in this case. Figure 6 describes the dependence of the UH, EM and WM modes on the product $K_Q K_S$. The growth rate increases with increasing coupling strength in a manner similar to the one shown by H86.

The value of K_Q used by H86 was estimated empirically making total precipitation proportional to SST anomalies. Since the wave convergence part has been taken care of separately in our study, K_Q should be less. Therefore, in figure 7, the dependence of the UH mode as well as the gravest eastward and westward propagating modes on q_s and four different strengths of K_Q for $k = 0{\cdot}15$ is shown. A point of interest in this figure is that with smaller strengths of K_Q the new unstable modes are excited only for larger strength of the convergence feedback. However, as the atmosphere approaches moist neutrality their growth rates increase exponentially. This character of dependence on q_s is seen for all wavelengths (i.e., all k). For $q_s > 0{\cdot}95$, the growth rates of some of the new unstable modes become comparable or even larger than that of the UH mode. It is to be noted that for moderate strength of convergence feedback, even if the coupling strength is one-quarter the strength used by Hirst (1986), the UH mode may be unstable and may still be the dominant mode. The dispersion relation for $q_s = 0{\cdot}98$ when K_Q is one tenths its standard strength is shown in figure 8. The mode numbered 6 is the UH mode. As in the standard case, we note that the unstable modes appear in two sets, one

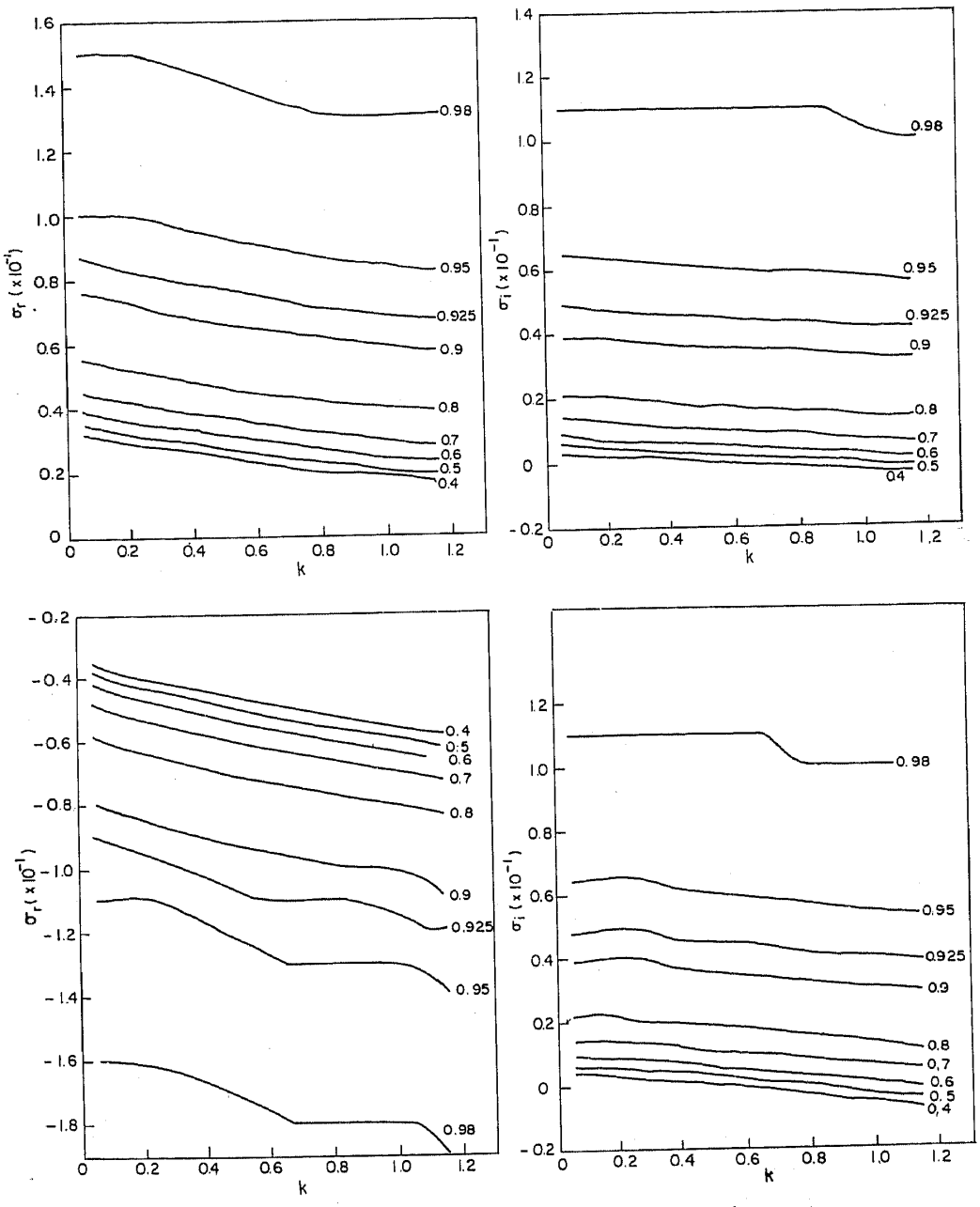

Figure 4. Same as in figure 3 for (**a**) EM mode and (**b**) WM mode.

eastward propagating and the other westward propagating. This shows that the behaviour of the modes for smaller K_Q is similar to that of the standard case except that the new unstable modes are excited for higher and higher strengths of convergence feedback. Since the characteristics of the dispersion relation remains qualitatively same even at small K_Q, we have used the standard K_Q for examining the structure and some sensitivity of these modes.

Note that the new modes were interannual modes in the absence of convergence feedback that become intraseasonal modes with increasing q_s (figure 5). For example, the periods of the gravest eastward and westward propagating new modes for $q_s = 0{\cdot}3$ and standard K_Q were 12 and 18 months. For $q_s = 0{\cdot}95$ they reduce to 3–4 months.

In order to derive some insight regarding the origin of the new unstable modes, the

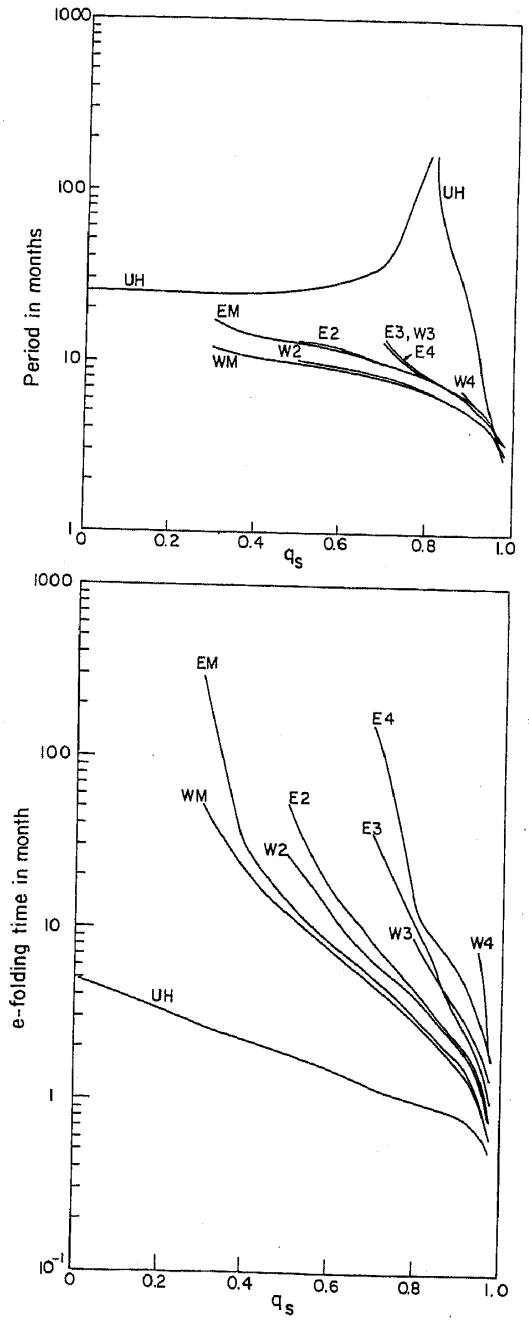

Figure 5. Dependence of the *e*-folding time and period of all the unstable modes on the strength of convergence feedback (q_s) for $k = 0{\cdot}15$.

dependence on the thermodynamic processes in the ocean is studied. Keeping the maximum value of $\bar{T}_x$ as $-5°C/10{,}000$ km (as in the standard case) the dependence of the nature of the unstable modes on fractions of $\bar{T}_x$ is studied i.e., the numbers 0·2, 0·4 etc. on the abscissa of figure 9 mean 0·2 times the standard value of $\bar{T}_x$, 0·4 times the standard value of $\bar{T}_x$ etc. Figure 9 shows the variation in the real and imaginary parts of the frequency for the UH mode and the gravest eastward and westward propagating modes as a function of $\bar{T}_x$ for three values of q_s and for $k = 0{\cdot}15$. It is seen that as $\bar{T}_x$ reduces the growth rates of the UH, EM and WM modes also reduce (for all three

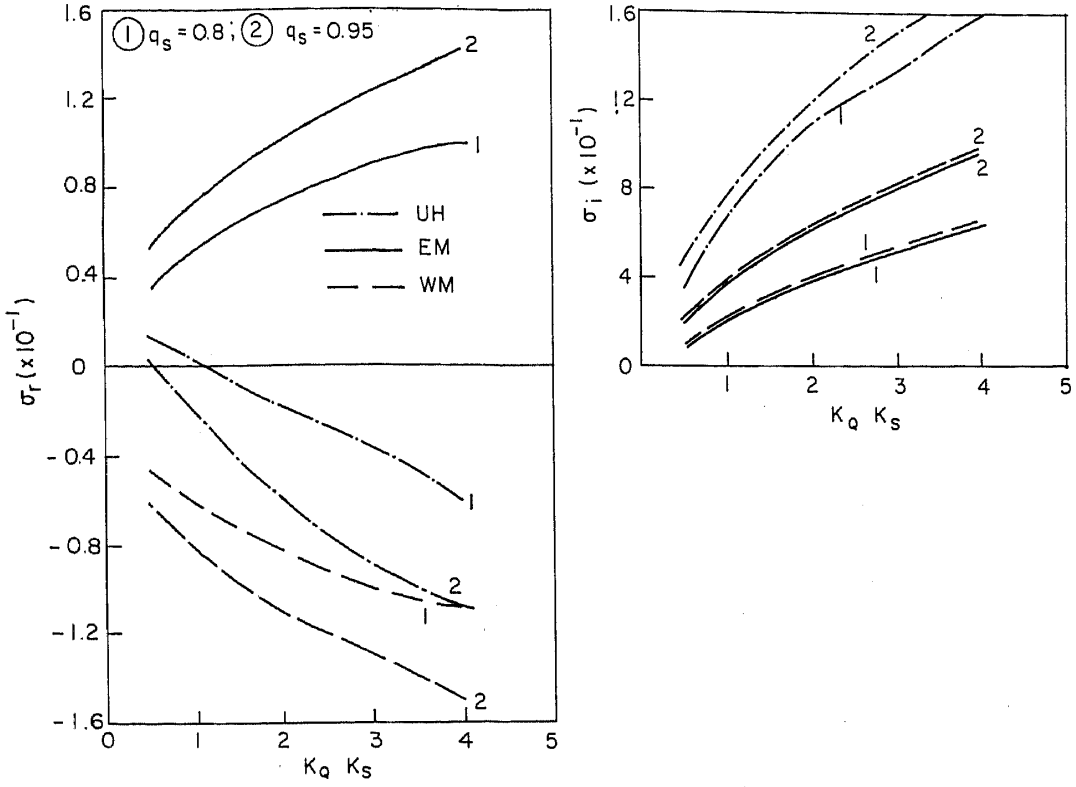

Figure 6. Dependence of the UH, EM and WM modes on coupling strength ($K_Q K_S$) at wavenumber $k = 0{\cdot}15$ for two different strengths of convergence feedback.

strengths of convergence feedback). The EM and WM modes become stable when $\bar{T}_x$ reduces below a critical value. Also, the growth rate and frequencies are larger for larger q_s and the critical value where the EM/WM modes stabilize is larger for larger q_s. However, for $q_s = 0{\cdot}4$ the EM/WM modes appear only when $\bar{T}_x$ is equal to the standard value. The change in behaviour of the real frequency of the UH mode with q_s is also clear. This implies that $\bar{T}_x$ is important for the new unstable modes. This in turn indicates that the advective processes in the ocean thermodynamics are crucial for the existence of the new unstable modes.

To further investigate how these modes depend on the thermodynamic processes governing the evolution of SST anomalies, the normal modes when the SST anomaly evolution is governed only by the upwelling (i.e., the 'upwelling' limit) and when the SST anomaly evolution is governed only by the advection of mean zonal SST gradient ($\bar{T}_x$) by the perturbation zonal currents (i.e., the 'advective' limit) are calculated.

4.1 *Upwelling limit*

If advective processes are unimportant ($\bar{T}_x = 0$ in equation (8d)) and upwelling is the dominant process present to determine the evolution of sea surface temperature anomalies it is found that the convergence feedback does not produce any new unstable modes. The only unstable mode present is the 'upwelling' mode similar to model I, IV of H86. Figure 10 shows the variation in the real and imaginary parts of the frequency as a function of wavenumber for different strengths of q_s. It can be seen that both the growth rate and the phase speed increase with increase in q_s. Also, the unstable region in the

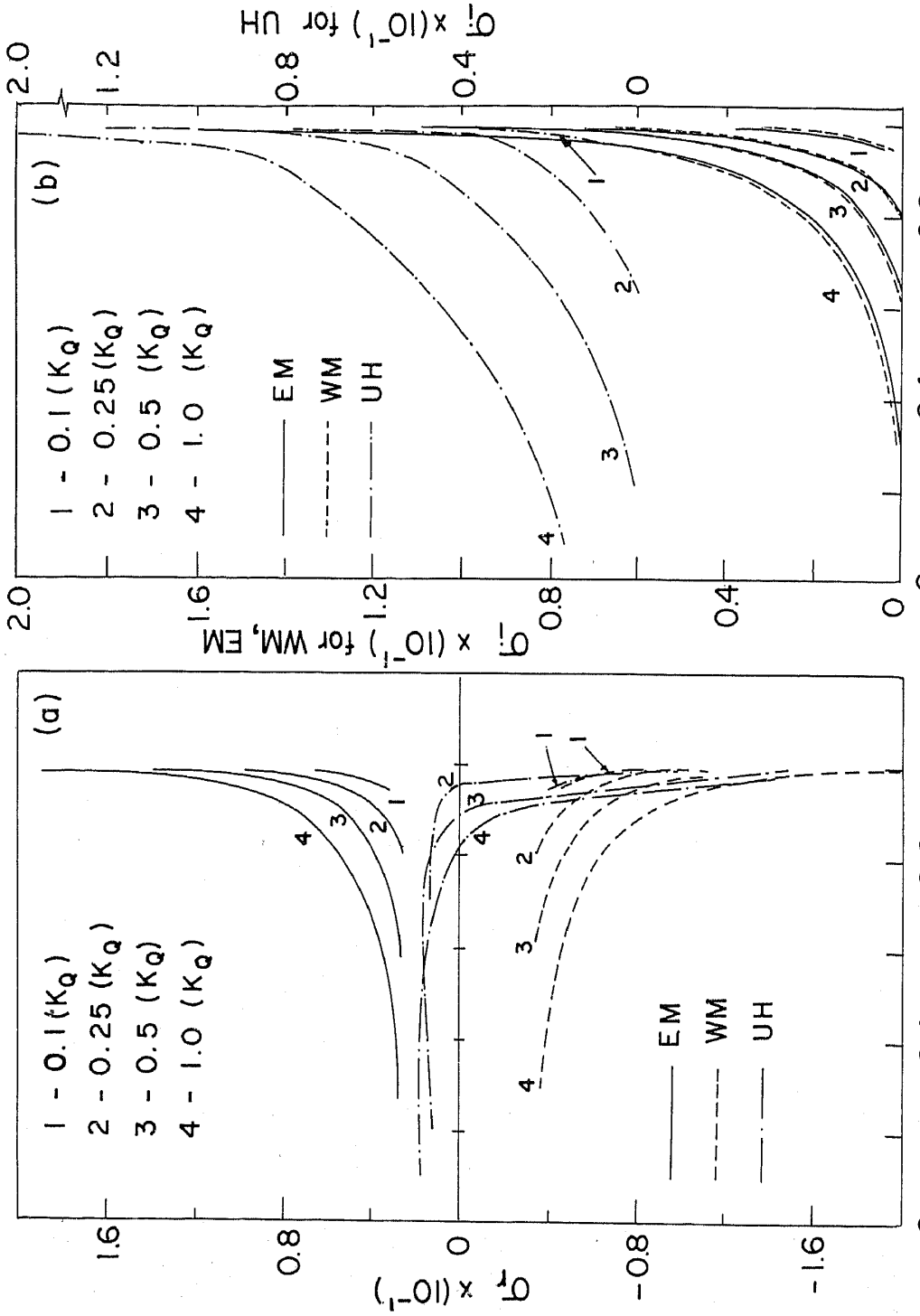

Figure 7. Dependence of real (σ_r) and imaginary (σ_i) frequencies of the three gravest modes on convergence feedback (q_s) for four strengths of K_Q at $k = 0{\cdot}15$.

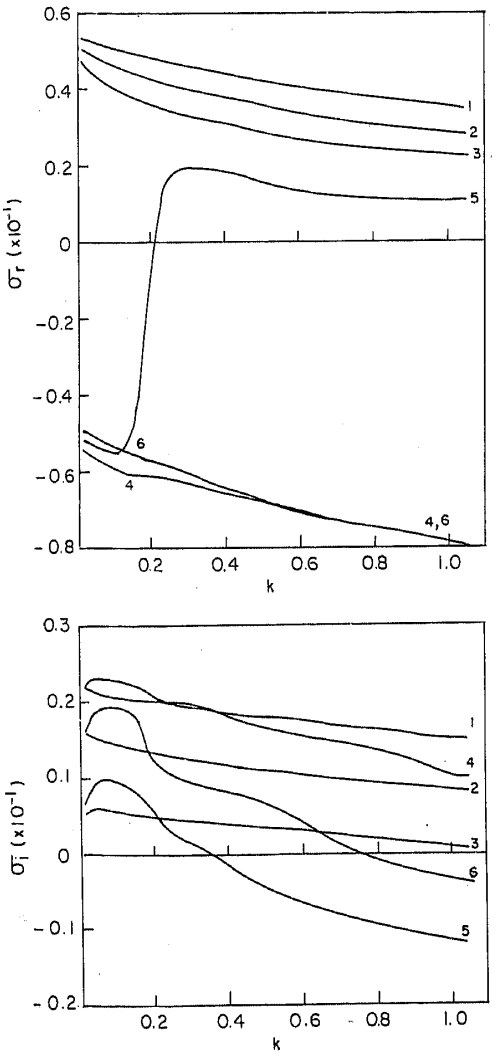

Figure 8. Non-dimensional dispersion relation (all modes) for $q_s = 0{\cdot}98$ for $K_Q = 0{\cdot}1(K_Q)$.

wavenumber domain increases with q_s. This model is similar to model IV of H86 and the mode shown in figure 10 is the same mode B of Hirst and Lau (1990) for their small C_a^* (i.e. our large q_s) and their large D_M (our A, B) case. It may be noted that in this parameter regime Hirst and Lau (1990) also get only one mode (mode B). When D_M (our A, B) is reduced considerably we also find three unstable modes as seen by them. Thus, in the upwelling limit our results are similar to theirs.

4.2 *Advective limit*

Similarly, if the upwelling is unimportant ($K_M = 0$ in equation (8d)), figure 11 shows the real and imaginary frequencies of all the unstable modes present when advection is the only thermodynamic process invoked to determine the evolution of SST anomalies in the presence of convergence feedback for $q_s = 0{\cdot}8$. The striking feature in the figure is the appearance of two classes of eastward and westward propagating modes somewhat similar to the general thermodynamic case. Only one unstable mode has a clear maximum like the UH mode in the general thermodynamic case. However, this mode is

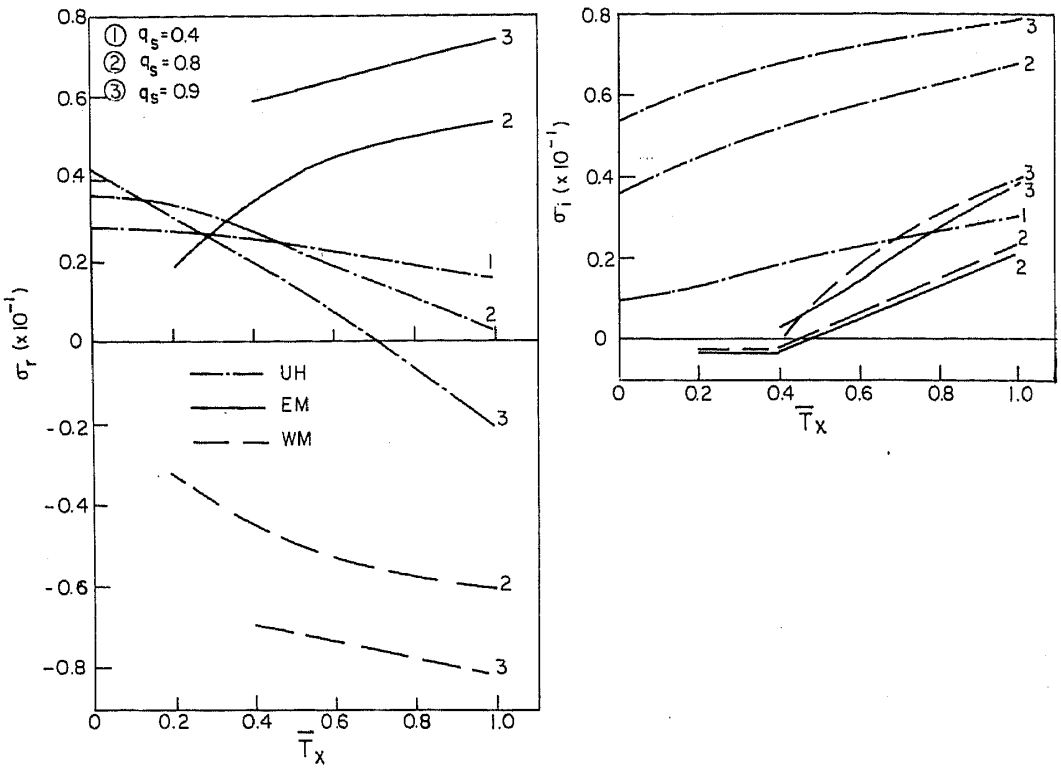

Figure 9. Dependence of the real and imaginary frequencies of the three gravest modes on $\overline{T}_x$ for three values of q_s.

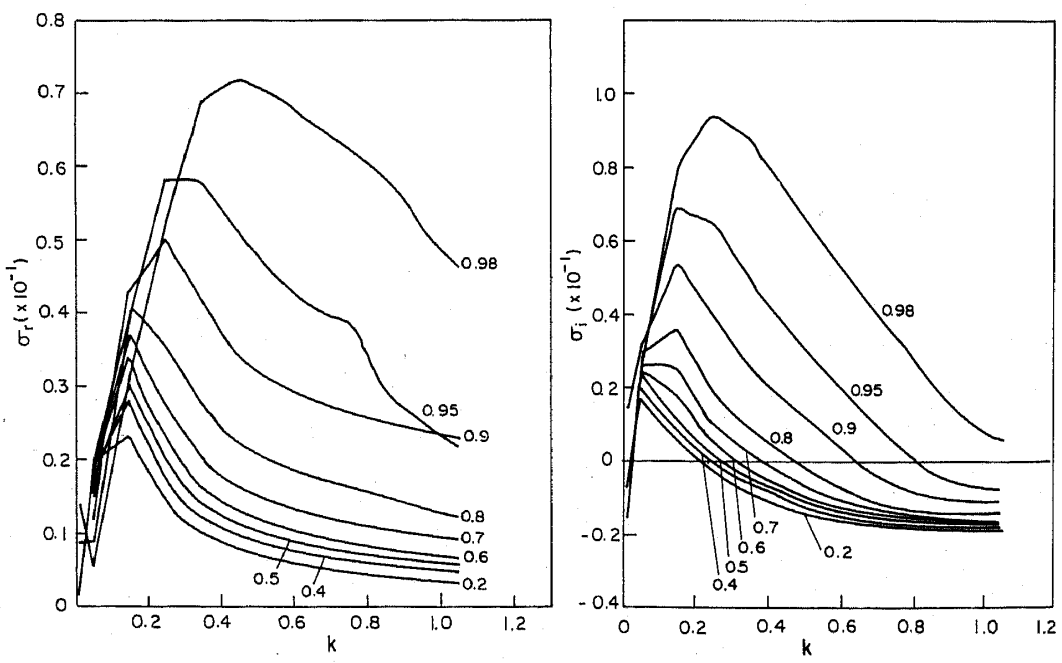

Figure 10. Non-dimensional dispersion relation for the "upwelling" only thermodynamic case. The dependence of the only unstable mode on the convergence feedback (q_s) is shown.

westward propagating for all wavenumbers. The presence of some upwelling seems to slow down this mode for small wavenumbers. Except this mode which has strong dependence on wavenumber, the other westward and eastward propagating unstable modes have very weak dependence on wavenumber similar to the new unstable modes

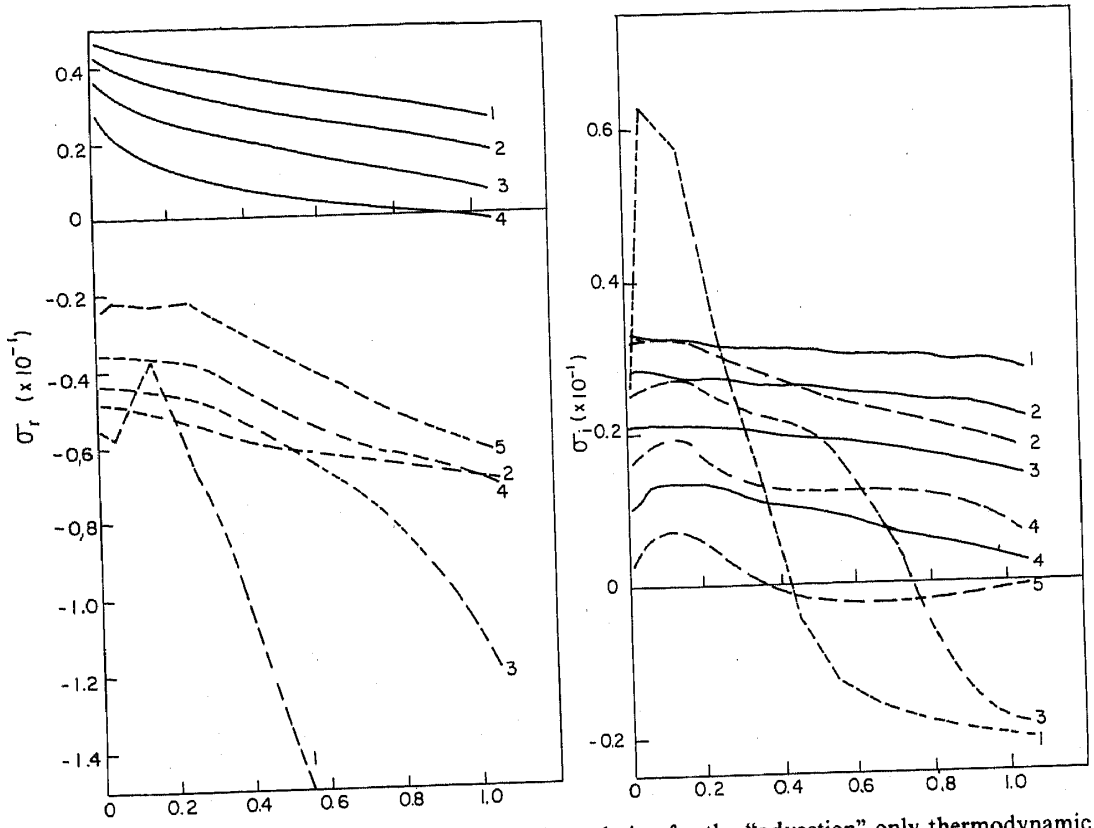

Figure 11. Non-dimensional dispersion relation for the "advection" only thermodynamic case for $q_s = 0{\cdot}8$ (all modes). Abscissa is wave number k.

in the general thermodynamic case. The fact that the two eastward and westward propagating new classes of unstable modes are present in the 'advective' limit but not in the 'upwelling' limit implies that these new modes that appear when convergence feedback is introduced are basically 'advective' modes and that upwelling is not necessary for their existence. As q_s is increased the growth rates of the eastward and westward moving modes increase more rapidly than those of the UH type mode and beyond a certain strength of convergence feedback ($q_s \approx 0{\cdot}95$) the growth rates of all the modes become comparable. In this limit Hirst and Lau (1990) found a mode (designated by them as mode A) whose structure crucially depends on the relative strength of C_a^* ($=(1-q_s)C_a$) and C_0. They showed that when $C_a^* > C_0$ the oceanic Rossby wave is destabilized and when $C_a < C_0$ the oceanic Kelvin wave is destabilized For the values of C_a^* used by Hirst and Lau (1990) the parameter q_s (in our notation) is $\geqslant 0{\cdot}9955$. Also the dissipation rates used by Hirst and Lau (1990) is much smaller than the ones used in our study. For values of $q_s > 0{\cdot}99$ and for smaller dissipation, we also get many unstable modes, one of which is similar to mode A of Hirst and Lau (1990). The modes discussed here are unstable even for lower values of q_s and in spite of high dissipation rates. Hence these are new modes and of a different type.

Hence it can be said that the unstable modes of the general thermodynamics case, the UH mode and the westward propagating modes, in particular, are basically advective modes that are influenced by upwelling.

It is to be noted that the atmosphere alone with convergence feedback ($q_s \leqslant 1$, in the absence of any other feedback like the evaporation-wind feedback) does not support any unstable normal mode. Thus, these unstable modes arise purely due to coupling

Table 2. Sign of the energy source terms for all the unstable modes for two values of q_s.

$q_s = 0{\cdot}8$				$q_s = 0{\cdot}95$			
Mode	$-\langle\theta T\rangle$	$-\langle Uu\rangle$	$-\langle Vv\rangle$	Mode	$-\langle\theta T\rangle$	$-\langle Uu\rangle$	$-\langle Vv\rangle$
UH	+	+	+	UH	+	+	−
WM	+	+	−	WM	+	+	−
W2	+	+	−	W2	+	+	−
W3	+	+	−	W3	+	+	−
EM	−	−	+	W4	+	+	−
E2	−	−	+	EM	−	−	+
E3	−	−	+	E2	−	−	+
E4	−	+	+	E3	−	−	+
				E4	+	+	−
				E5	+	+	+

between the atmosphere and the ocean. Convergence feedback introduces new coupled unstable modes through the following process. The modified atmospheric heating field, due to the inclusion of convergence feedback, modifies the eigenfunctions for some modes in such a way that the correlations between the lower layer atmospheric winds and ocean currents may now be positive, leading to the growth of ocean perturbations. From the eigenfunctions of all the unstable modes the sign of the source terms in the energy integral was calculated. The signs of the source terms for all the unstable modes for $q_s = 0{\cdot}8$ and $q_s = 0{\cdot}95$ are shown in table 2. This shows that the convergence feedback makes either or both the terms involving correlation between surface winds and ocean currents ($-\langle uU\rangle$, $-\langle vV\rangle$) positive for the new unstable modes.

Figure 12 shows the structure of the eigenfunction for the UH mode when $q_s = 0{\cdot}8$. It is seen that the θ-field and U-field of the atmosphere and the h-field and u-field of the ocean do not coincide. The shift in phase actually determines the direction of propagation. It can be seen that the maximum positive temperature perturbation, the maximum positive ocean u-current perturbation and maximum negative zonal wind perturbations coincide (the sign of the atmospheric wind is opposite to that of ocean current since in the model positive U represents upper level wind). But the convergence field and the negative θ perturbation fields are ahead by a little less than half a cycle. This arrangement helps in the sustenance of the instability since it is such that winds drawn into the convergence field from both sides overlie positive low-level wind perturbations to the west of the convergence maximum and very weak positive low-level wind perturbations to the east. This results in an eastward movement of the perturbation. Also, the convergence in the atmosphere coincides with the positive maximum thermocline depth anomaly in the ocean.

The structure of the maximally unstable eastward propagating and westward propagating (EM and WM) modes is very different from that of the UH mode and it can be seen from figures 13 and 14 that they possess higher meridional structures. As discussed earlier, these modes are all coupled modes and as a result their meridional structure may not resemble that of any neutral normal mode.

Since the new eastward and westward propagating waves remain eastward and westward propagating respectively even when q_s is increased (figure 4), their

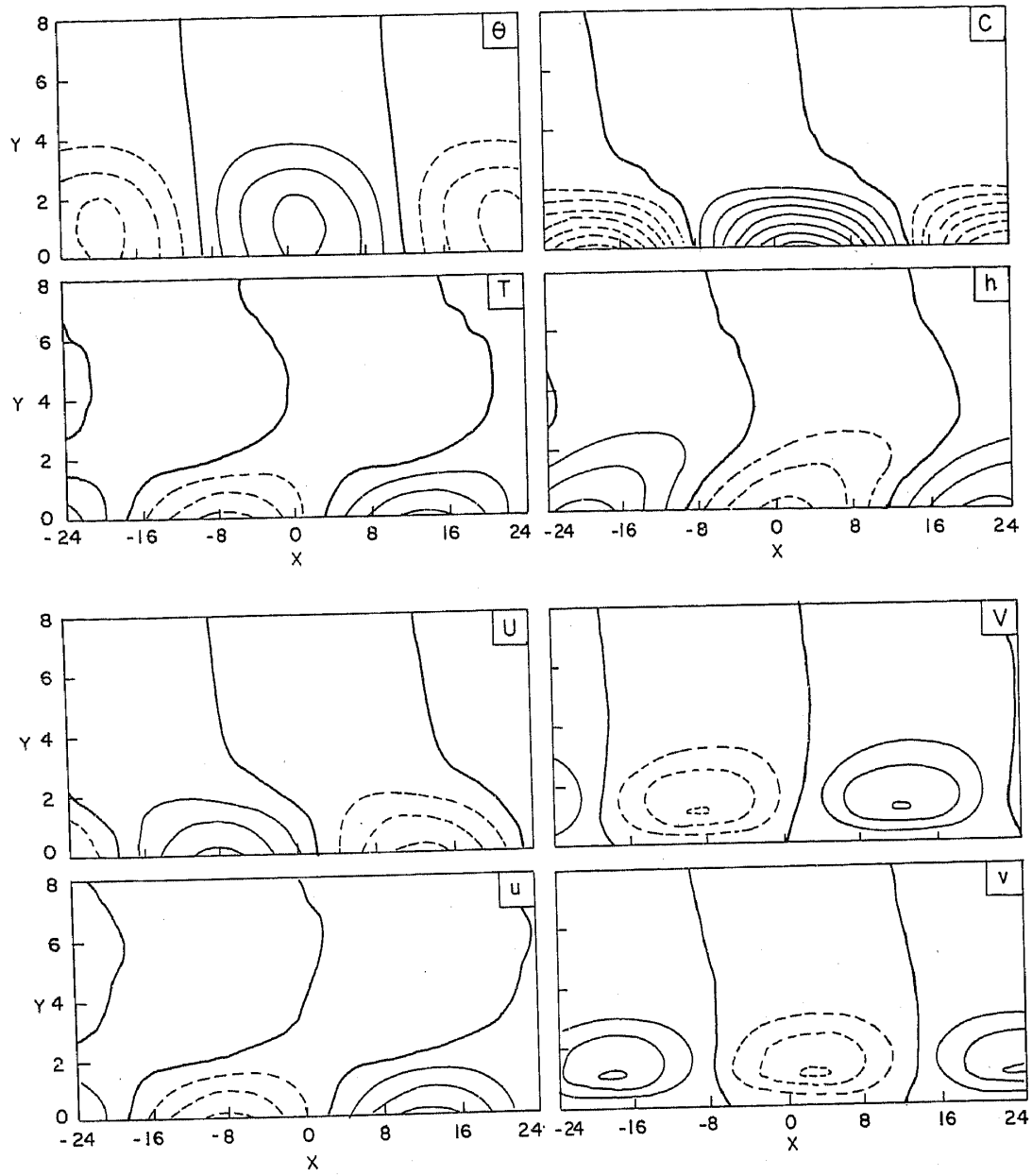

Figure 12. Non-dimensional eigenfunctions for the UH mode for $q_s = 0{\cdot}8$ at $k = 0{\cdot}15$. 0·9, 0·6, and 0·3 of the maximum values are contoured for all the variables except the upper level convergence denoted by C. C is calculated using the normalized values of U and V. For C the minimum contour is 0·02 and the contour interval is 0·02. The zero line is thick solid, positive lines are thin solid and negative lines are dashed.

eigenfunctions also remain similar. However, as q_s increases, the UH mode changes its character (figure 3). Therefore, the structure of the UH mode in the westward propagating regime ($k = 0{\cdot}15$ and $q_s = 0{\cdot}95$) is also shown in figure 15. In this case, the maximum positive anomaly of ocean temperature coincides with the maximum anomalous atmospheric convergence and the maximum negative θ perturbation. The collocation of these variables helps in the maintenance and growth of the instability. But the maximum positive anomalous oceanic zonal current u lies behind by about a quarter of a cycle and the low-level positive atmospheric zonal wind U lies behind by about half a cycle. This arrangement results in westward propagation.

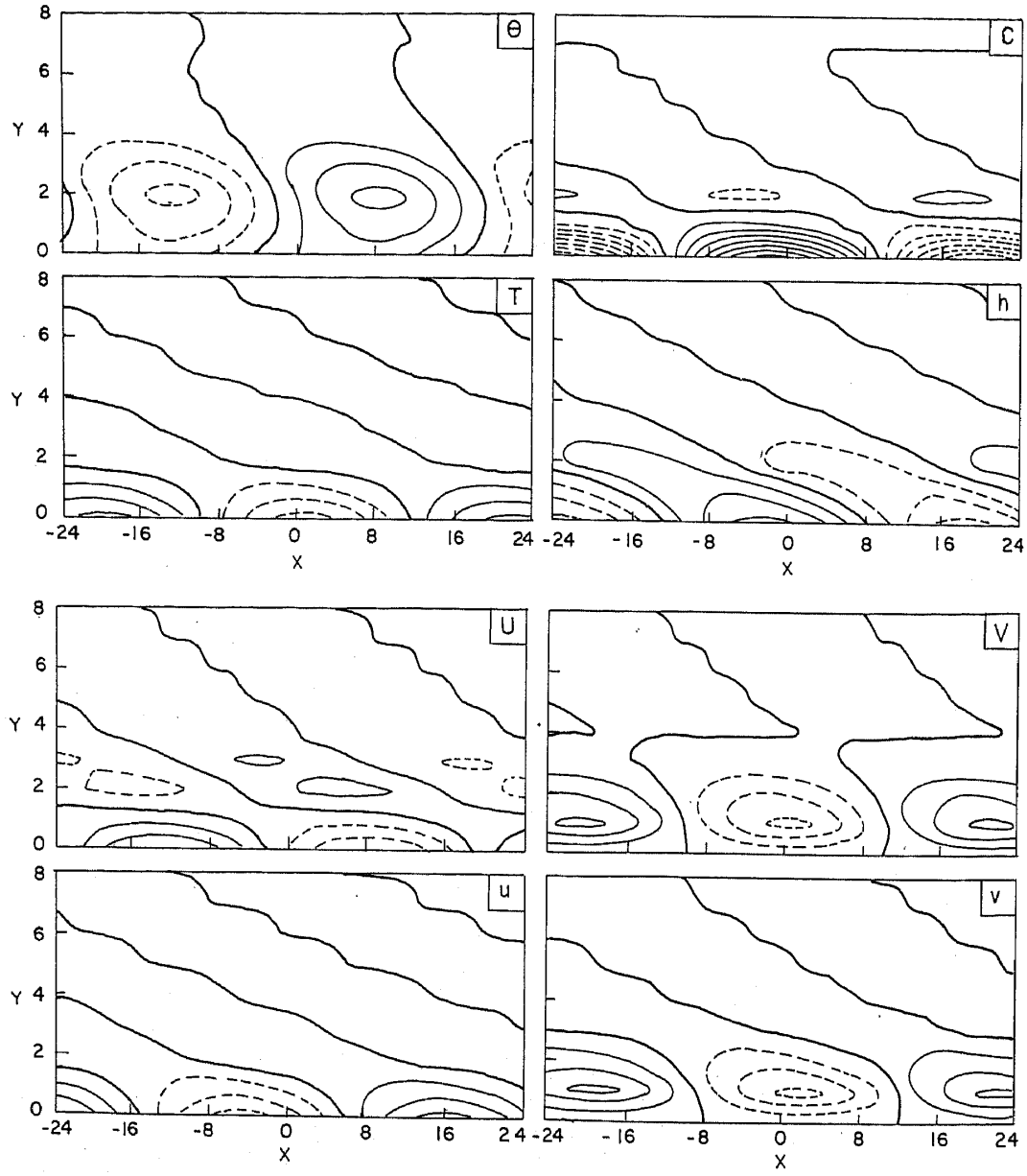

Figure 13. Same as in figure 12 for the WM mode.

5. Conclusions

It is argued that the convergence feedback (or wave-CISK) is important in determining the atmospheric heating in the tropics and that it introduces some significant effects on the coupled tropical normal modes. First of all, the growth rate of the only unstable mode, that was present in the absence of convergence feedback, increases drastically with the increase in the strength of convergence feedback. The phase speed of this most unstable eastward propagating mode (UH mode) decreases with increase in the strength of convergence feedback until it becomes stationary at $q_s \simeq 0{\cdot}8$. Beyond this value of q_s it becomes westward propagating. This is significant, as it may explain why some ENSO anomalies propagate slowly to the east while some others propagate

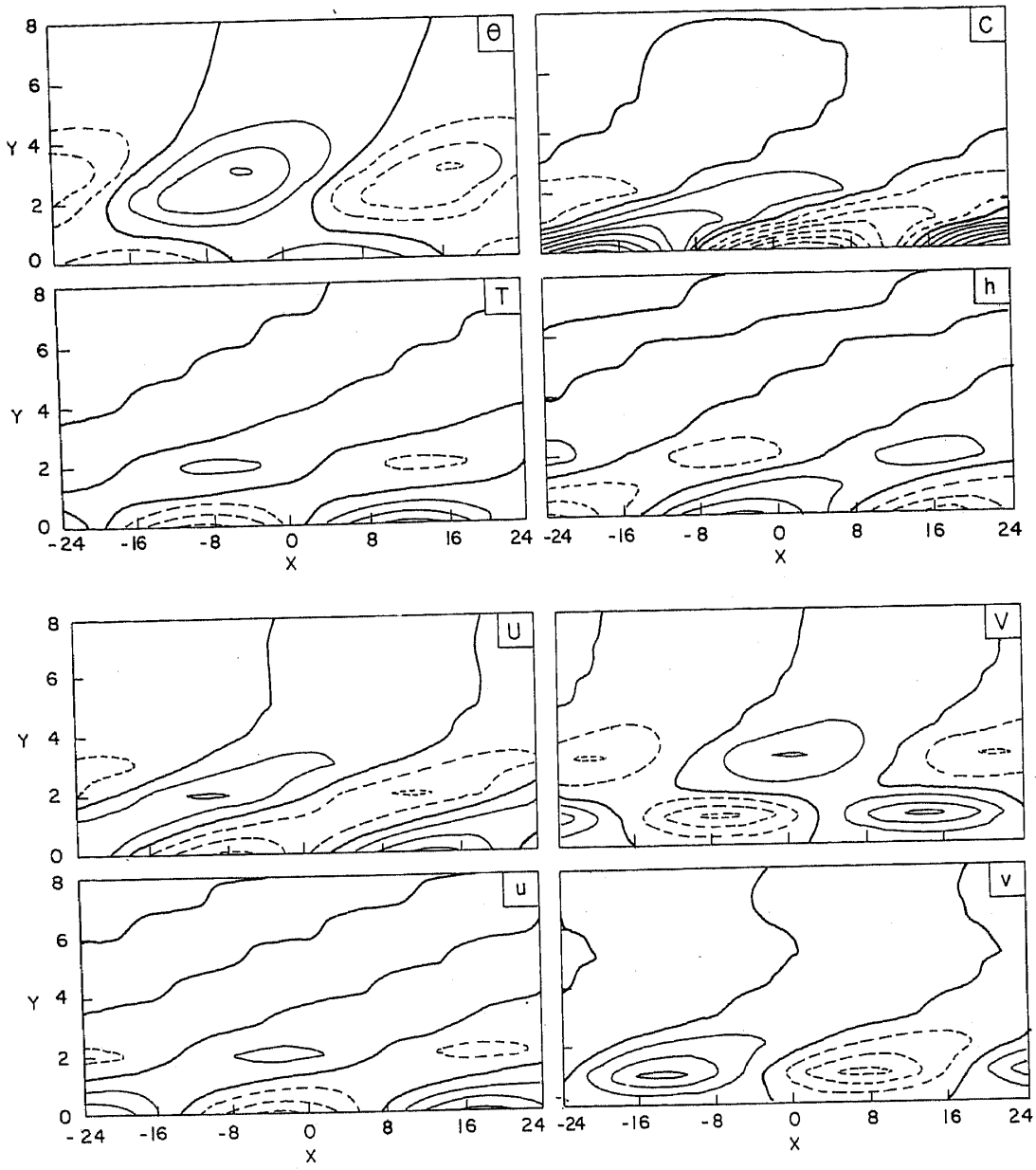

Figure 14. Same as in figure 12 for the EM mode.

slowly to the west. Moreover, in the absence of the convergence feedback, the maximally growing UH mode has a wavelength of about 10,000 km (H86), nearly twice as large as that of the ENSO anomalies. With reasonable strength of convergence feedback, the maximum growth of the UH mode occurs for wavelengths 5000–6000 km (figure 3). This agrees much better with the observed ENSO anomalies. Additionally, several new unstable modes are introduced if the strength of convergence feedback exceeds a critical value. Some of these modes are eastward-propagating, while some others are westward-propagating. For moderate values of the strength of convergence feedback ($q_s \leqslant 0{\cdot}95$), the growth rates of the new modes are smaller than that of the UH mode but their growth rates can be even larger than that of the UH mode when the atmosphere is close to the moist neutral state ($q_s \simeq 1{\cdot}0$). In the absence of convergence feedback these modes are neutral interannual modes with periods greater than one

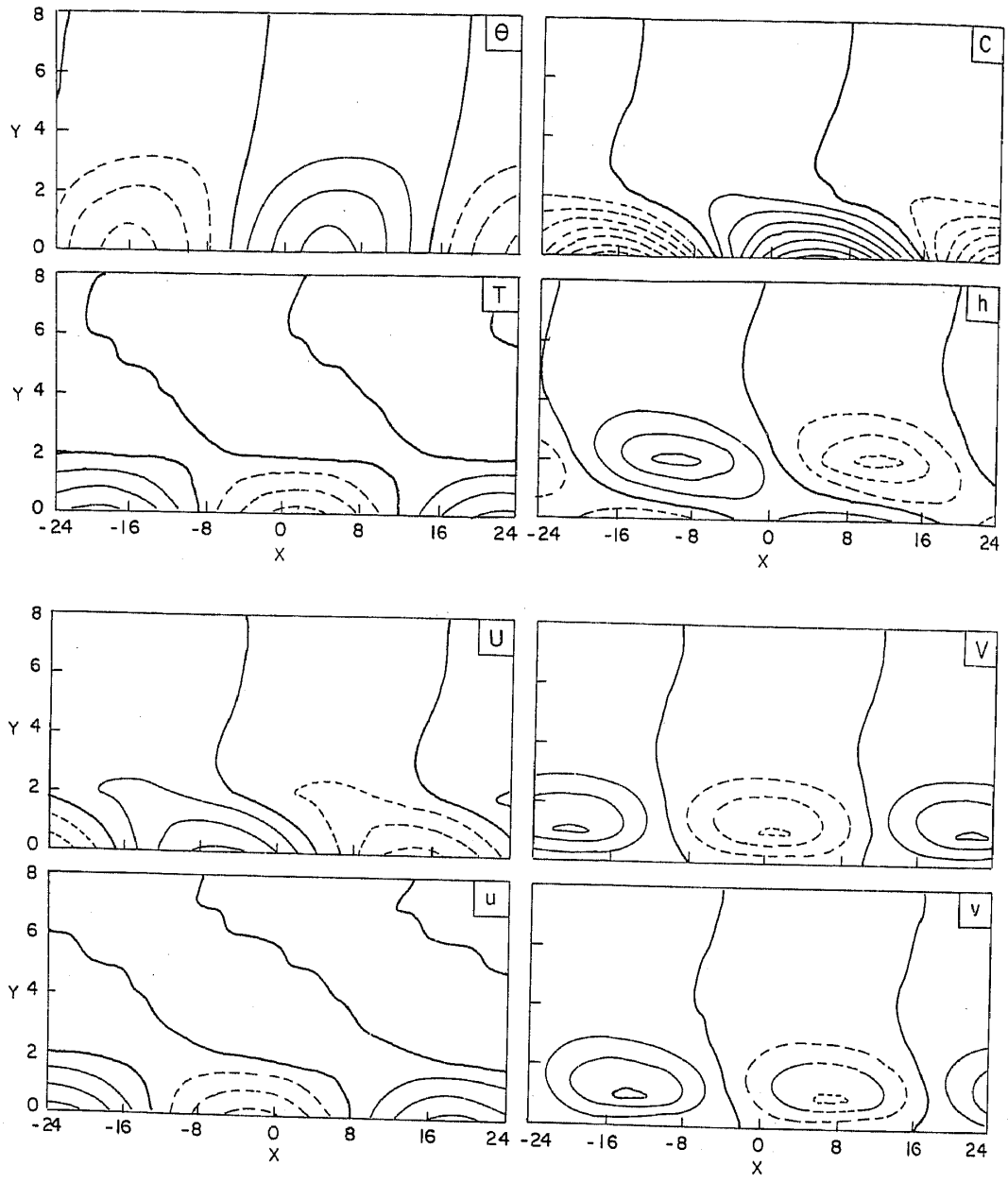

Figure 15. Same as in figure 12 for $q_S = 0{\cdot}95$.

year. The convergence feedback increases their real frequencies and makes them intraseasonal modes for reasonable values of q_s. It is also shown that these modes are basically 'advective' modes that are partially influenced by upwelling.

The new unstable modes would basically introduce a background 'noise' in the system as their growth rates do not selectively depend on a particular scale. As long as the largest growth rate of the UH mode is greater than that of these modes, it would be possible to identify this dominant signal (i.e., the ENSO signal). Since the dimensional q_s depends nonlinearly on the background mean SST, the non-dimensional q_s would be much closer to unity in the western Pacific while it would be much smaller in the eastern Pacific. Thus, we expect the new unstable modes to be present in the western part of the Pacific but they would be absent or very weak in the eastern Pacific.

These results may also explain some of the differences between individual warm events. The growth rates of individual warm events are quite different (e.g., figure 1·18 of Philander 1990). For example, the 1982–83 event was triggered sometime during the middle of the calendar year but grew explosively. It is to be noted that the growth rate of the UH mode depends rather sensitively on the strength of the convergence feedback (or on mean SST). Thus, the differences in growth rates of the warm events may be due to differences in the mean SST distributions prior to the triggering of such events. These results may also explain aspects of variabilities of some more complex coupled models. For example, the coupled model of Zebiak and Cane (1987) simulates many features of the ENSO variability including the dominant periodicity embedded in an aperiodic background. Recently, Goswami and Shukla (1991b) showed that aperiodicity in the standard version of the Zebiak and Cane's model arises primarily due to the convergence feedback. In view of these results it is possible that the aperiodicity in the Zebiak and Cane's model is due to the rather broad band and relatively weak unstable modes introduced by the convergence feedback. It is also hypothesized that the aperiodicity of the observed ENSO cycle may be due to the interaction between the dominant ENSO mode with weakly unstable broad band modes generated by the convergence feedback.

Appendix. Rational for selection of basis functions and truncation

The basic equations (8) and properties of parabolic cylinder functions demand that if U, θ, u, h, T are expressed with symmetric parabolic cylinder functions, V and v must be

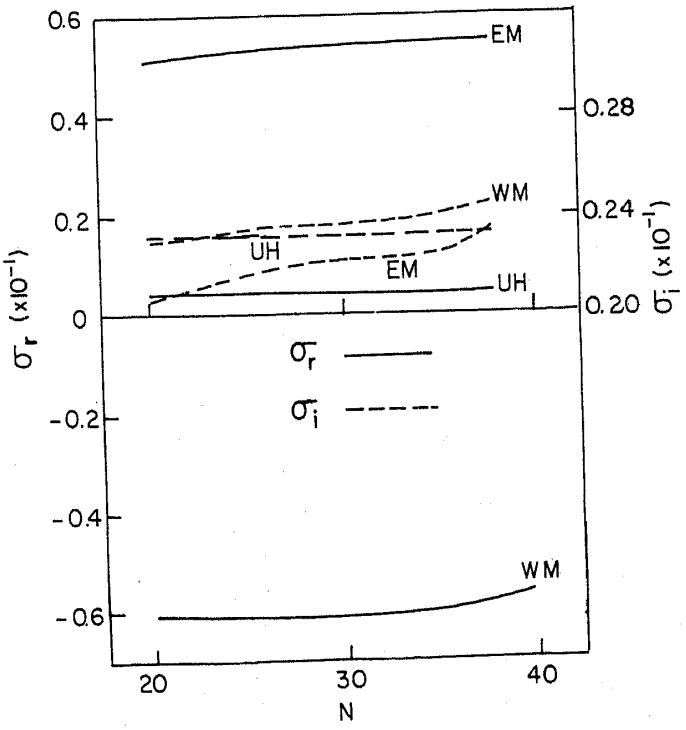

Figure 16. Dependence of the real and imaginary frequencies on N (Number of parabolic cylinder functions) of the UH, EM and WM modes for $q_s = 0{\cdot}98$ at $k = 0{\cdot}15$. The scale for the imaginary frequencies is highly expanded.

expressed in terms of antisymmetric ones and vice versa. In our study, we have expressed U, θ, u, h, T by symmetric and V, v by antisymmetric functions. We also examined whether any of the modes with antisymmetric U, θ, u, h, T and symmetric V, v are unstable. It is found that these modes are always stable. Hence our choice of symmetric basis functions for U, θ, u, h, T and antisymmetric basis functions for V and v.

Although the series was truncated at $N = 20$ for the results presented here, a test of convergence was carried out to evaluate the degree of convergence of the low-frequency modes of interest as N is increased beyond 20. As shown in figure 16, the real and imaginary frequencies of these modes at low wave numbers do not change appreciably after $N = 20$. Note that the scale for the imaginary frequencies is highly expanded. This provides a rationale for truncation at $N = 20$.

Acknowledgements

We wish to thank Prof. M Sankar Rao for encouragement throughout this work. We also thank Ms K Nagarathna for her help in the preparation of the manuscript. This work was supported by the Department of Ocean Development, India.

References

Battisti D S and Hirst A C 1989 Interannual variability in the tropical atmosphere/ocean system: Influence of the basic state and ocean geometry; *J. Atmos. Sci.* **46** 1687–1712

Davey M K and Gill A E 1987 Experiments on tropical circulation with a simple moist model; *Q. J. R. Meteorol. Soc.* **113** 1237–1269

Fennessy M J, Marx L and Shukla J 1985 GCM sensitivities to 1982–83 equatorial Pacific sea surface temperature anomalies; in *Coupled ocean atmosphere models* (ed.) JCJ Nihoul *Elsevier Oceanogr. Sci.* **40** 121–130

Goswami B N and Shukla J 1991a Predictability of a coupled ocean-atmosphere model; *J. Climate* **4** 3–22

Goswami B N and Shukla J 1991b Aperiodic variability of the Cane-Zebiak model; A diagnostic study; (*J. Climate*) (submitted)

Goswami B N and Selvarajan S 1991 Convergence feedback and unstable low frequency oscillations in a simple coupled ocean-atmosphere model; *Geophys. Res. Lett.* **18** 991–994

Hirst A C 1986 Unstable and damped equatorial modes in simple coupled ocean-atmosphere models; *J. Atmos. Sci.* **43** 606–630

Hirst A C and Lau K M 1990 Intraseasonal and interannual oscillations in coupled ocean-atmosphere models: *J. Climate* **3** 713–725

Lau K M and Shen S 1988 On the dynamics of intraseasonal oscillations and ENSO; *J. Atmos. Sci.* **45** 1781–1797

Philander S G H 1990 *El Nino, La Nina and the Southern Oscillation* (Academic Press) pp 289

Philander S G H, Yamagata T and Pacanowski R C 1984 Unstable air-sea interactions in the tropics; *J. Atmos. Sci.* **41** 604–613

Rennick M A and Haney R 1986 Stable and unstable air-sea interactions in the equatorial region; *J. Atmos. Sci.* **43** 2937–2943

Shukla J and Wallace J M 1983 Numerical simulation of the atmospheric response to equatorial Pacific sea surface temperature anomalies; *J. Atmos. Sci.* **40** 1613–1630

Suarez M J and Schopf P S 1988 A delayed action oscillator for ENSO; *J. Atmos. Sci.* **45** 3283–3287

Webster P J 1981 Mechanisms determining the atmospheric response to sea surface temperature anomalies; *J. Atmos. Sci.* **38** 554–571

Yamagata T 1985 Stability of a simple air-sea coupled model in the tropics. In *Coupled ocean atmosphere models* (ed.) J C J Nihoul *Elsevier Oceanogr. Sci.* **40** 637–658

Zebiak S E 1982 A simple atmospheric model of relevance to El Nino; *J. Atmos. Sci.* **39** 2017–2027

Zebiak S E and Cane M A 1987 A model of El Nino°Southern Oscillation; *Mon. Weath. Rev.* **115** 2262–2278